

Pavel Loiko, Josep Maria Serres, Xavier Mateos, Magdalena Aguiló, Francesc Díaz, Lizhen Zhang, Zhoubin Lin, Haifeng Lin, Ge Zhang, Konstantin Yumashev, Valentin Petrov, Uwe Griebner, Yicheng Wang, Sun Yung Choi, Fabian Rotermund, and Weidong Chen, "Monoclinic $\text{Tm}^{3+}:\text{MgWO}_4$: a promising crystal for continuous-wave and passively Q-switched lasers at $\sim 2 \mu\text{m}$," *Opt. Lett.* 42, 1177-1180 (2017)

Monoclinic $\text{Tm}^{3+}:\text{MgWO}_4$: A novel crystal for continuous-wave and passively Q-switched lasers at $\sim 2 \mu\text{m}$

PAVEL LOIKO,^{1,2} JOSEP MARIA SERRES,¹ XAVIER MATEOS,^{1,4,*} MAGDALENA AGUILÓ,¹ FRANCESC DÍAZ,¹ LIZHEN ZHANG,³ ZHOUBIN LIN,³ HAIFENG LIN,³ GE ZHANG,³ KONSTANTIN YUMASHEV,⁵ VALENTIN PETROV,⁴ UWE GRIEBNER,⁴ YICHENG WANG,⁴ SUN YUNG CHOI,⁶ FABIAN ROTERMUND,⁷ AND WEIDONG CHEN,^{3,4,**}

¹*Física i Cristal·lografia de Materials i Nanomaterials (FiCMA-FiCNA), Universitat Rovira i Virgili (URV), Campus Sescelades, c/ Marcel·lí Domingo, s/n., E-43007 Tarragona, Spain*

²*ITMO University, 49 Kronverkskiy pr., 197101 St. Petersburg, Russia*

³*Key Laboratory of Optoelectronic Materials Chemistry and Physics, Fujian Institute of Research on the Structure of Matter, Chinese Academy of Sciences, Fuzhou, 350002 Fujian, China*

⁴*Max Born Institute for Nonlinear Optics and Short Pulse Spectroscopy, Max-Born-Str. 2a, D-12489 Berlin, Germany*

⁵*Center for Optical Materials and Technologies, Belarusian National Technical University, 65/17 Nezavisimosti Ave., 220013 Minsk, Belarus*

⁶*Department of Energy Systems Research, Ajou University, 16499 Suwon, Republic of Korea*

⁷*Department of Physics, KAIST, 291 Daehak-ro, Yuseong-gu, 34141 Daejeon, South Korea*

*Corresponding author: xavier.mateos@urv.cat, mateos@mbi-berlin.de

**e-mail: chenweidong@fjirsm.ac.cn

Received XX Month XXXX; revised XX Month, XXXX; accepted XX Month XXXX; posted XX Month XXXX (Doc. ID XXXXX); published XX Month XXXX

Monoclinic thulium-doped magnesium monotungstate, $\text{Tm}^{3+}:\text{MgWO}_4$, is promising for efficient power-scalable continuous-wave (CW) and passively Q-switched lasers at $>2 \mu\text{m}$. Under diode-pumping at 802 nm, a compact CW laser based on Z-cut $\text{Tm}:\text{MgWO}_4$ generated 3.09 W at 2022-2034 nm with a slope efficiency of 50% which represents the highest output power ever achieved with this type of laser host. Stable passive Q-switching of the $\text{Tm}:\text{MgWO}_4$ laser is demonstrated for the first time using single-walled carbon nanotubes (SWCNTs), graphene and $\text{Cr}^{2+}:\text{ZnS}$ saturable absorbers. Using the latter best performance are achieved with 16.1 μJ / 13.6 ns pulses at 2017.8 nm with to

a maximum average output power of 0.87 W and a peak power of 1.18 kW.

OCIS codes: (140.3380) Laser materials; (140.3580) Lasers, solid state; (140.3540) Lasers, Q-switched.

<http://dx.doi.org/10.1364/OL.99.099999>

Tungstate crystals doped with rare-earth (RE) ions, e.g. Nd^{3+} , Yb^{3+} , Tm^{3+} , or Ho^{3+} represent an important class of laser-active materials [1]. A most prominent example is the family of monoclinic double tungstates (MDTs) with chemical formula $\text{KRE}(\text{WO}_4)_2$ where RE = Gd, Y or Lu. During the last decade, RE-doped MDTs with ordered structure have been extensively

studied for the development of highly efficient near-IR lasers [2]. MDTs offer a strong anisotropy, broad and intense spectral bands for the RE³⁺ ions and minimal fluorescence quenching. They are Raman-active and possess suitable thermo-optic properties. The family of the divalent-metal monotungstate crystals with wolframite structure and chemical formula M²⁺WO₄ where M²⁺ is Mg, Mn, Co, Ni, Zn, Cd is known for long time but has not been actively exploited for hosting laser active ions yet [3-5]. Monoclinic disordered MWO₄ crystals were studied as scintillators [6] and Raman shifters [4]. In contrast to the MDTs, these monotungstates do not contain passive RE ions and doping with laser-active REs are obviously be more difficult.

MgWO₄ (called huanzalaite when found as a mineral) is monoclinic (point group *2/m*, space group *P2/c*, lattice constants $a = 4.686 \text{ \AA}$, $b = 5.675 \text{ \AA}$, $c = 4.928 \text{ \AA}$, $\beta = a \wedge c = 90.3^\circ$, $Z = 2$) [3,7]. The wolframite type structure of MgWO₄ is described as a network of interconnected zigzag chains of alternate MgO₆ and WO₆ distorted octahedra along the *c*-axis [3,4]. The Mg²⁺ cations are distributed over two non-equivalent sites with a distorted VI-fold O²⁻ coordination. MgWO₄ is optically biaxial. The principal refractive indices are still unknown and the assignment of the optical indicatrix axes {X, Y, Z} in MgWO₄ is arbitrary [8]. There exist only rough data on the average refractive index *n* of MgWO₄ ($n \sim 2.1$). It should be noted that the thermal conductivity of MgWO₄ ($\sim 8.7 \text{ W/mK}$) is almost 3 times larger than that of MDTs [9].

When MgWO₄ is doped with RE³⁺ ions, they substitute for the Mg²⁺ ones. The charge compensation is achieved by Mg²⁺ vacancies or the various-valence impurity cations entering the interstitial positions [10,11]. The distortion of the crystal field for the RE³⁺ ions is facilitated by a significant difference in ionic radii of Mg²⁺ (0.72 Å) and the RE³⁺ dopant (e.g., for Tm³⁺, the ionic radius is 0.88 Å). As a consequence, one can expect strongly anisotropic and broadband absorption and emission properties from the RE³⁺-doped MgWO₄ crystals.

Cr³⁺ doped MgWO₄ has been grown and described in the literature but no laser operation has been reported for this transition metal dopant yet [12]. Systematic study of optical spectroscopy and laser operation of RE³⁺-doped MgWO₄ has been carried out only for Yb³⁺ [8]. Under diode-pumping, a maximum output power of 2.52 W at 1060 nm was generated in the continuous wave (CW) regime with a slope efficiency of $\sim 53\%$. The thulium ion (Tm³⁺) is attractive due to its broadband emission around $\sim 2 \mu\text{m}$ (the ³F₄ \rightarrow ³H₆ transition) which makes Tm lasers suitable for remote sensing and medical applications. The present work is devoted to Tm³⁺-doped MgWO₄. Power scaling of a CW Tm:MgWO₄ laser and its passive Q-switching with various saturable absorbers are demonstrated for the first time.

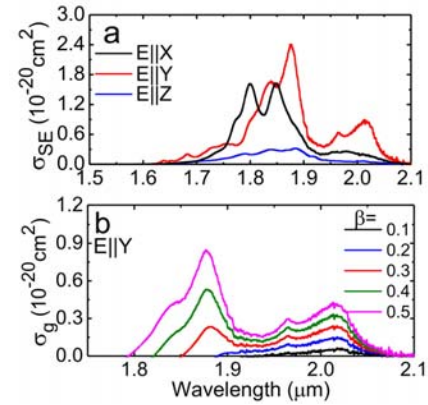


Fig. 1. Spectroscopy of Tm³⁺ in monoclinic MgWO₄: (a) stimulated-emission cross-sections, σ_{SE} , for the principal light polarizations $E \parallel X$, Y and Z ; (b) gain cross-sections, $\sigma_g = \beta\sigma_{SE} - (1-\beta)\sigma_{abs}$, for light polarization $E \parallel Y$ (³F₄ \rightarrow ³H₆ transition of Tm³⁺, inversion ratio $\beta = N(^3F_4)/N_{Tm}$).

The spectroscopy of Tm:MgWO₄ has been studied very recently [13]. Tm:MgWO₄ possesses a broad absorption band related to the ³H₆ \rightarrow ³H₄ transition which is suitable for pumping with AlGaAs diodes. The maximum absorption cross-section σ_{abs} is $2.04 \times 10^{-20} \text{ cm}^2$ at 802.6 nm for $E \parallel X$. For the ³F₄ \rightarrow ³H₆ transition corresponding to the 2 μm laser operation, a strong anisotropy of the stimulated-emission cross-sections (σ_{SE}), is observed, as shown in Fig. 1(a). This strong anisotropy implies a natural selection of a linear polarization of the laser emission. The largest σ_{SE} of $2.43 \times 10^{-20} \text{ cm}^2$ is at 1877 nm and corresponds to $E \parallel Y$. Thus, the X-cut and Z-cut crystals are interesting for laser operation. The gain cross-section spectra ($\sigma_g = \beta\sigma_{SE} - (1-\beta)\sigma_{abs}$) for $E \parallel Y$, exhibit a local maximum at $\sim 2.02 \mu\text{m}$ even at low inversion ratios β , see Fig. 1(b), which makes Tm:MgWO₄ promising for laser operation at wavelengths longer than 2 μm . In contrast, the gain maximum of Tm³⁺-doped MDTs is typically around 1.9 μm [2].

The Tm:MgWO₄ crystal was grown by the Top-Seeded Solution Growth (TSSG) method using Na₂WO₄ as a flux. The actual Tm concentration in the crystal was $1.41 \times 10^{20} \text{ cm}^{-3}$ corresponding to 0.89 at.%. From the as-grown crystal, a rectangular sample was cut in the optical indicatrix frame with dimensions 1.86(X) \times 3.96(Y) \times 3.05(Z) mm³. It was polished from all sides to laser quality and remained uncoated. Two crystal orientations (X-cut and Z-cut) were tested.

At first, we studied the CW performance of the Tm:MgWO₄ laser. The experiments were performed in a microchip-type cavity, see details in [14]. The laser crystal was mounted in a water cooled (14°C) Cu-holder. Indium foil was used to provide a better thermal contact between laser and Cu-holder. A plano-plano cavity was composed of a flat pump mirror (PM) antireflection (AR) coated for 0.77-1.05 μm and high reflection (HR) coated for 1.80-2.08 μm , and a flat output coupler (OC) with transmission of $T_{oc} = 0.1\%$, 1.5%, 3%, 5% or 9% at 1.84-2.1 μm . Both the PM and OC were placed as close as possible to the

crystal. The laser crystal was pumped through the PM by a fiber-coupled AlGaAs laser diode (fiber core diameter: 200 μm , N.A.: 0.22) emitting unpolarized radiation at ~ 802 nm. To collimate and focus the pump light we used an AR-coated lens assembly (focal length: 30 mm, 1:1 imaging ratio). The radius of the pump beam in the crystal was 100 μm (beam quality factor $M^2 = 86$, confocal parameter of the pump beam $2z_R = 1.9$ mm). The OCs provided a partial reflection ($R \sim 40\%$) at the pump wavelength. The total pump absorption under lasing conditions was 14% and 30% for the X-cut and Z-cut, respectively, as determined based on the pump-transmission measurement under non-lasing conditions and the rate equations.

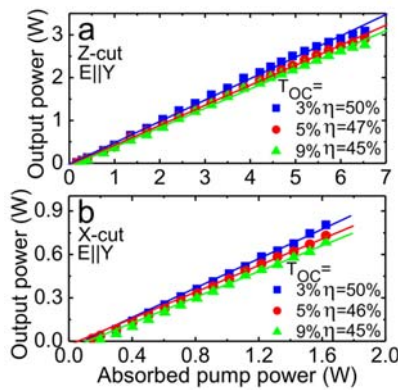


Fig. 2. Input-output characteristics of CW Tm:MgWO₄ lasers based on Z-cut (a) and X-cut (b) crystals, η - slope efficiency.

The power scaling characteristics of the CW Tm:MgWO₄ lasers are shown in Fig. 2. For both crystal cuts, the laser output was linearly polarized, $E \parallel Y$, in agreement with Fig. 1(a). For the Z-cut crystal, the maximum output power was 3.09 W at 2022–2034 nm (multi-peak spectra due to etalon effects) corresponding to a slope efficiency of $\eta = 50\%$ (with respect to the absorbed pump power, P_{abs}) for $T_{\text{OC}} = 3\%$. The laser threshold was at $P_{\text{abs}} = 0.18$ W and the optical-to-optical efficiency with respect to the incident power was 14%. At $P_{\text{abs}} > 6$ W, a roll-over of the output dependences was observed. It can be attributed to thermal effects or the decrease of the mode-matching efficiency for the pump and laser beams under the condition of a strong thermal lens [14]. However, no thermal fracture of the crystal was observed. For the X-cut crystal, similar values of η were achieved but the power scaling was limited by its low absorption.

By changing the OC, a spectral tunability in the 2020–2057 nm range was observed, Fig. 3. For high T_{OC} , laser oscillation occurred at ~ 2.02 μm in agreement with the gain cross-section spectra, see Fig. 1(b). The red-shift of the laser wavelength with decreasing T_{OC} is due to the quasi-three-level nature of the Tm³⁺ laser.

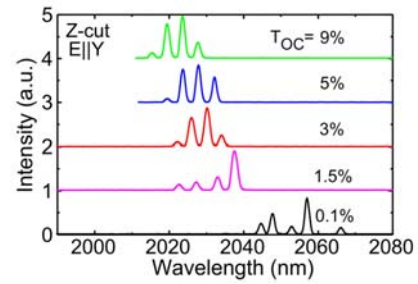


Fig. 3. Typical laser spectra from the Tm:MgWO₄ laser for various transmissions of the output coupler (T_{OC}), $P_{\text{abs}} = 6$ W.

Passively Q-switched (PQS) Tm:MgWO₄ lasers were realized using a Z-cut oriented crystal because of the best performance in CW operation. A set of saturable absorbers (SA) was studied: (i) 2.21 mm-thick AR-coated polycrystalline Cr²⁺:ZnS SA (IPG Photonics) with a small-signal transmission $T_{\text{SA}} = 88.9\%$, (ii) a commercial graphene-SA (Graphenea) containing 3 carbon layers with $T_{\text{SA}} = 94.4\%$, produced by the CVD method, and (iii) a custom-made SA based on single-walled carbon nanotubes (SWCNTs) with $T_{\text{SA}} = 97.9\%$, fabricated by the arc-discharged method and randomly oriented in a 300 nm-thick PMMA film [15]. The T_{SA} values are specified at the laser wavelength. The graphene and SWCNT-SAs were deposited on uncoated 1.05 mm-thick quartz substrates. Carbon nanostructures have attracted a lot of attention during the recent years due to their broadband and ultrafast saturable absorption [15,16]. Cr²⁺:ZnS is a well-recognized SA for PQS of Tm lasers featuring high pulse energies [17,18]. The SA was inserted between the crystal and OC with minimum air gaps.

A fast InGaAs photodiode with 200 ps rise time (Alphasal, model UPD-5N-IR2-P), and a 2 GHz digital oscilloscope (Tektronix DPO5204B) were used for monitoring the Q-switched pulses.

Stable passive Q-switching was achieved with all three SAs. The laser output was linearly polarized, $E \parallel Y$. The input-output dependences of the PQS Tm:MgWO₄ lasers are shown in Fig. 4(a,b). For the Cr²⁺:ZnS SA, the maximum average output power reached 872 mW at 1717.8 nm corresponding to $\eta = 23\%$ and a conversion efficiency with respect to the CW mode $\eta_{\text{conv}} = 47\%$. The laser operated with $T_{\text{OC}} = 9\%$ and emitted a single-peak spectrum, see Fig. 4(c). Further power scaling was limited by optical damage of the SA. For the SAs based on carbon nanostructures, the power scaling was limited by the Q-switching instabilities induced by heating of the SA by the residual pump [19]. $T_{\text{OC}} = 5\%$ was selected for the PQS lasers based on carbon nanostructures. For SWCNT-SA, the laser generated 317 mW at 2006–2021 nm with a multi-peak spectrum, Fig. 4(d), $\eta = 22\%$ and $\eta_{\text{conv}} = 39\%$. When using graphene-SA, only 274 mW were extracted at shorter wavelengths, 2012–2015 nm with lower $\eta = 18\%$ and $\eta_{\text{conv}} = 30\%$. This lower efficiency is connected with a shift of the spectral emission to shorter

wavelengths, 2012–2015 nm, an indication of higher insertion loss of the graphene-SA.

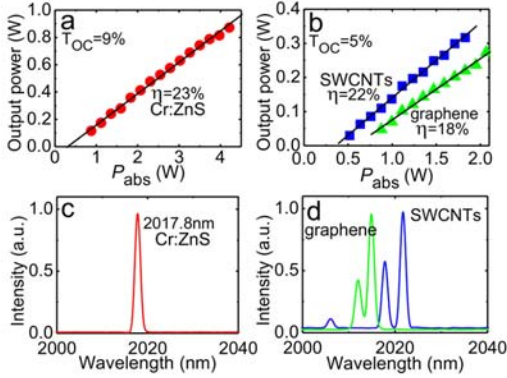


Fig. 4. Input-output characteristics (a,b) and laser spectra (c,d) for the Tm:MgWO₄ lasers PQS with Cr²⁺:ZnS SA (a,c) and graphene-SA and SWCNT-SA (b,d): η – slope efficiency. The spectra are recorded at $P_{\text{abs}} = 4$ W (c) and at $P_{\text{abs}} = 1.7$ W (d). The crystal is Z-cut, $E \parallel Y$.

Using the Cr²⁺:ZnS-SA, the pulse characteristics of the PQS Tm: MgWO₄ laser (energy E_{out} and duration $\Delta\tau$, the latter calculated as a full width at half maximum, FWHM) were weakly dependent on P_{abs} , see Fig. 5(a,c). This behaviour is typical for “slow” SAs [20]. At $P_{\text{abs}} = 4.21$ W, the laser generated 16.1 μJ / 13.6 ns pulses at a pulse repetition frequency (PRF) of 54.2 kHz. As a result, the peak power $P_{\text{peak}} = E_{\text{out}}/\Delta\tau$ reached 1.18 kW.

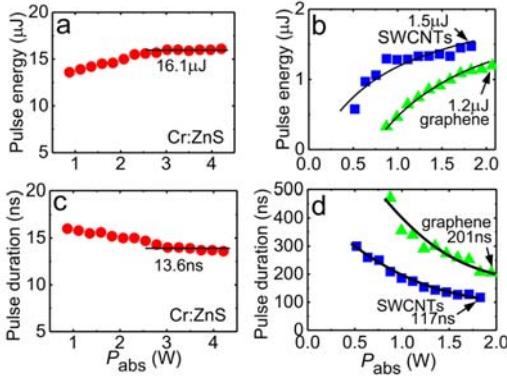


Fig. 5. Tm:MgWO₄ lasers PQS with Cr²⁺:ZnS SA (a,c), graphene-SA and SWCNT-SA (b,d): pulse energy (a,b), and pulse duration, FWHM (c,d). P_{abs} – absorbed pump power. The laser crystal is Z-cut, $E \parallel Y$.

For the “fast” SAs based on carbon nanostructures (graphene and SWCNTs), the pulse characteristics of the Tm:MgWO₄ laser were dependent on the pump level, Fig. 5(b,d). Using the SWCNT-SA, 1.5 μJ / 117 ns pulses were achieved at PRF = 215 kHz. These parameters outperform those achieved with the graphene-SA (1.2 μJ / 201 ns pulses at PRF = 229 kHz) due to the lower fraction of the nonsaturable losses and, hence, higher modulation depth for the SWCNT-SA [21]. The corresponding maximum peak power reached 12.6 W and 6.0 W for the

SWCNT-SA and the graphene-SA based PQS laser, respectively. The output characteristics of the PQS Tm:MgWO₄ lasers are summarized in Table 1.

The oscilloscope records of the shortest Q-switched pulses and typical pulse trains generated by the PQS Tm:MgWO₄ lasers are shown in Fig. 6. The intensity fluctuations in the pulse train were <5% and <10% and the rms pulse-to-pulse timing jitter was <7% and <15% for the Cr²⁺:ZnS and SWCNT-SA, respectively.

Table 1 Output Characteristics of the PQS Tm:MgWO₄ Lasers

SA	P_{out} , mW	η , %	η_{conv} , %	E_{out} , μJ	$\Delta\tau$, ns	PRF, kHz	P_{peak} , W
Cr ²⁺ :ZnS	872	23	47	16.1	13.6	54.2	1184
SWCNT	317	22	39	1.5	117	215	12.6
Graphene	274	18	30	1.2	201	229	6.0

P_{out} – average output power, η – slope efficiency, η_{conv} – Q-switching conversion efficiency, E_{out} – pulse energy, $\Delta\tau$ – pulse duration (FWHM), PRF – pulse repetition frequency, P_{peak} – peak power.

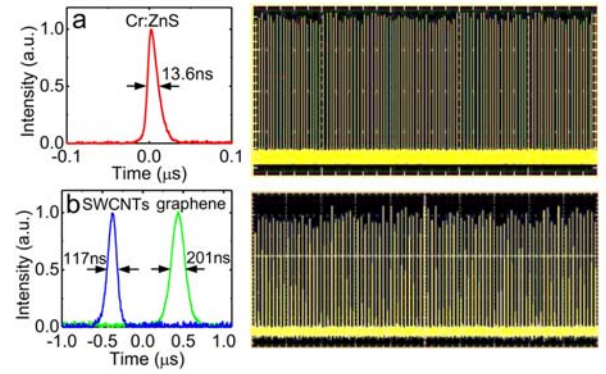


Fig. 6. Oscilloscope traces of the Tm:MgWO₄ laser PQS by Cr²⁺:ZnS (a), graphene-SA and SWCNT-SA (b). (a) *left* – single pulse measured at $P_{\text{abs}} = 4.21$ W, *right* – pulse train at $P_{\text{abs}} = 1.8$ W, the total time span is 5 ms, PRF = 24 kHz; (b) *left* – single pulses measured at $P_{\text{abs}} = 1.83$ W (SWCNT-SA) and at 2.07 W (graphene-SA), *right* – pulse train for SWCNT-SA at $P_{\text{abs}} = 1.6$ W, the total time span is 500 μs , PRF = 197 kHz.

In conclusion, we report on power scaling of a diode-pumped Tm:MgWO₄ laser reaching ~3 W of output power at ~2.03 μm with a slope efficiency of 50% which is comparable to the best results achieved with Tm³⁺-doped MDTs in similar setups, see e.g. Ref. [14]. Microchip laser operation with X-cut and Z-cut crystals is demonstrated indicating a positive thermal lens in this crystal [14]. Stable passive Q-switching of the Tm:MgWO₄ laser with Cr²⁺:ZnS, graphene- and SWCNT-SAs is realized for the first time. Doping MgWO₄ with higher Tm³⁺ concentration (few at.%) is potentially interesting for highly-efficient multi-watt CW and PQS lasers operating at wavelengths slightly above 2 μm . Tm:MgWO₄ is a candidate for ultrashort pulse mode-locked lasers due to its broad and smooth gain profile both for the $E \parallel Y$ and $E \parallel X$ polarizations.

Funding. Spanish Government (MAT2016-75716-C2-1-R, MAT2013-47395-C4-4-R, TEC 2014-55948-R); Generalitat de Catalunya (2014SGR1358), National Natural Science Foundation of China (11404332, 61575199, 21427801), Key Project of Science and Technology of Fujian Province (2016H0045), the Strategic Priority Research Program of the Chinese Academy of Sciences (XDB20000000); the National Key Research and Development Program of China (2016YFB0701002), the China Scholarship Council (CSC, 201504910418 and 201504910629), the Instrument project of Chinese Academy of Sciences (YZ201414).

Acknowledgment. F.D. acknowledges additional support through the ICREA academia award 2010ICREA-02 for excellence in research. This work has received funding from the European Union's Horizon 2020 research and innovation programme under grant agreement No 654148 Laserlab-Europe and under the Marie Skłodowska-Curie grant agreement No 657630. P.L. acknowledges financial support from the Government of the Russian Federation (Grant 074-U01) through ITMO Post-Doctoral Fellowship scheme.

References

1. A. A. Kaminskii, *Laser & Photon. Rev.* **1**, 93 (2007).
2. V. Petrov, M. C. Pujol, X. Mateos, O. Silvestre, S. Rivier, M. Aguiló, R. Solé, J. Liu, U. Griebner, and F. Díaz, *Laser & Photon. Rev.* **1**, 179 (2007).
3. E. Cavalli, A. Belletti, and M. G. Brik, *J. Phys. Chem. Solids* **69**, 29 (2008).
4. P. Becker, L. Bohaty, H. J. Eichler, H. Rhee, and A.A. Kaminskii, *Laser Phys. Lett.* **4**, 884 (2007).
5. F. G. Yang, C. Y. Tu, H. Y. Wang, Y. P. Wei, Z. Y. You, G. H. Jia, J. F. Li, Z. J. Zhu, X. A. Lu, and Y. Wang, *J. Alloys Compd.* **455**, 269 (2008).
6. F. A. Danevich, D. M. Chernyak, A. M. Dubovik, B. V. Grinyov, S. Henry, H. Kraus, V. M. Kudovbenko, V. B. Mikhailik, L. L. Nagornaya, R. B. Podviyanuk, O. G. Polischuk, I. A. Tupitsyna, and Y. Y. Vostretsov, *Nucl. Instrum. Meth. A* **608**, 107 (2009).
7. V. B. Kravchenko, *J. Struct. Chem.* **10**, 139 (1969).
8. L. Zhang, W. Chen, J. Lu, H. Lin, L. Li, G. Wang, G. Zhang, and Z. Lin, *Opt. Mater. Express* **6**, 1627 (2016).
9. L. Zhang, Y. Huang, S. Sun, F. Yuan, Z. Lin, and G. Wang, *J. Lumin.* **169**, Part A, 161 (2016).
10. A. Lupei, V. Lupei, C. Gheorghe, L. Gheorghe, and A. Achim, *J. Appl. Phys.* **104**, 083102 (2008).
11. W. Kolbe, K. Petermann, and G. Huber, *IEEE J. Quantum Electron.* **21**, 1596 (1985).
12. L. Y. Li, Y. Yu, G. F. Wang, L. Z. Zhang, and Z. B. Lin, *Cryst. Eng. Comm.* **15**, 6083 (2013).
13. L.Z. Zhang, Z.B. Lin, H.F. Lin, G. Zhang, X. Mateos, P. Loiko, J. M. Serres, M. Aguiló, F. Díaz, Y.C. Wang, V. Petrov, U. Griebner, E. Vilejshikova, K. Yumashev, and W.D. Chen, submitted to *Opt. Express* (2016).
14. J. M. Serres, X. Mateos, P. Loiko, K. Yumashev, N. Kuleshov, V. Petrov, U. Griebner, M. Aguiló, and F. Díaz, *Opt. Lett.* **39**, 4247 (2014).
15. W. B. Cho, J. H. Yim, S. Y. Choi, S. Lee, A. Schmidt, G. Steinmeyer, U. Griebner, V. Petrov, D.-I. Yeom, K. Kim, and F. Rotermund, *Adv. Funct. Mater.* **20**, 1937 (2010).
16. Q. Bao, H. Zhang, Y. Wang, Z. Ni, Y. Yan, Z. X. Shen, K. P. Loh, and D. Y. Tang, *Adv. Funct. Mater.* **19**, 3077 (2009).
17. M. Segura, M. Kadankov, X. Mateos, M. C. Pujol, J. J. Carvajal, M. Aguiló, F. Díaz, U. Griebner, and V. Petrov, *Opt. Express* **20**, 3394 (2012).
18. H. Yu, V. Petrov, U. Griebner, D. Parisi, S. Veronesi, and M. Tonelli, *Opt. Lett.* **37**, 2544 (2012).
19. J.M. Serres, P. Loiko, X. Mateos, K. Yumashev, U. Griebner, V. Petrov, M. Aguiló, and F. Díaz, *Opt. Express* **23**, 14108 (2015).
20. P. Loiko, J.M. Serres, X. Mateos, K. Yumashev, A. Yasukevich, V. Petrov, U. Griebner, M. Aguiló, and F. Díaz, *Opt. Lett.* **40**, 5220 (2015).
21. R. Lan, P. Loiko, X. Mateos, Y. Wang, J. Li, Y. Pan, S. Y. Choi, M. H. Kim, F. Rotermund, A. Yasukevich, K. Yumashev, U. Griebner, and V. Petrov, *Appl. Opt.* **55**, 4877 (2016).

References

1. A. A. Kaminskii, Laser crystals and ceramics: recent advances, *Laser & Photon. Rev.* **1**, 93 (2007).
2. V. Petrov, M. C. Pujol, X. Mateos, Ò. Silvestre, S. Rivier, M. Aguiló, R. Solé, J. Liu, U. Griebner, and F. Díaz, Growth and properties of $\text{KLu}(\text{WO}_4)_2$ and novel ytterbium and thulium lasers based on this monoclinic crystalline host, *Laser & Photon. Rev.* **1**, 179 (2007).
3. E. Cavalli, A. Belletti, and M. G. Brik, Optical spectra and energy levels of the Cr^{3+} ions in MWO_4 (M= Mg, Zn, Cd) and MgMoO_4 crystals, *J. Phys. Chem. Solids* **69**, 29 (2008).
4. P. Becker, L. Bohaty, H. J. Eichler, H. Rhee, and A.A. Kaminskii, High-gain Raman induced multiple Stokes and anti-Stokes generation in monoclinic multiferroic MnWO_4 single crystals, *Laser Phys. Lett.* **4**, 884 (2007).
5. F. G. Yang, C. Y. Tu, H. Y. Wang, Y. P. Wei, Z. Y. You, G. H. Jia, J. F. Li, Z. J. Zhu, X. A. Lu, and Y. Wang, Growth and spectroscopy of $\text{ZnWO}_4:\text{Ho}^{3+}$ crystal, *J. Alloys Compd.* **455**, 269 (2008).
6. F. A. Danevich, D. M. Chernyak, A. M. Dubovik, B. V. Grinyov, S. Henry, H. Kraus, V. M. Kudovbenko, V. B. Mikhailik, L. L. Nagornaya, R. B. Podviyanuk, O. G. Polischuk, I. A. Tupitsyna, and Y. Y. Vostretsov, MgWO_4 – a new crystal scintillator, *Nucl. Instrum. Meth. A* **608**, 107 (2009).
7. V. B. Kravchenko, Crystal structure of the monoclinic form of magnesium tungstate MgWO_4 , *J. Struct. Chem.* **10**, 139 (1969).
8. L. Zhang, W. Chen, J. Lu, H. Lin, L. Li, G. Wang, G. Zhang, and Z. Lin, Characterization of growth, optical properties, and laser performance of monoclinic $\text{Yb}:\text{MgWO}_4$ crystal, *Opt. Mater. Express* **6**, 1627 (2016).
9. L. Zhang, Y. Huang, S. Sun, F. Yuan, Z. Lin, and G. Wang, Thermal and spectral characterization of $\text{Cr}^{3+}:\text{MgWO}_4$ – a promising tunable laser material, *J. Lumin.* **169**, Part A, 161 (2016).
10. A. Lupei, V. Lupei, C. Gheorghe, L. Gheorghe, and A. Achim, Multicenter structure of the optical spectra and the charge-compensation mechanisms in $\text{Nd}:\text{SrWO}_4$ laser crystals, *J. Appl. Phys.* **104**, 083102 (2008).
11. W. Kolbe, K. Petermann, and G. Huber, Broadband emission and laser action of Cr^{3+} doped zinc tungstate at 1 μm wavelength, *IEEE J. Quantum Electron.* **21**, 1596 (1985).
12. L. Y. Li, Y. Yu, G. F. Wang, L. Z. Zhang, and Z. B. Lin, Crystal growth, spectral properties and crystal field analysis of $\text{Cr}^{3+}:\text{MgWO}_4$, *Cryst. Eng. Comm.* **15**, 6083 (2013).
13. L.Z. Zhang, Z.B. Lin, H.F. Lin, G. Zhang, X. Mateos, P. Loiko, J. M. Serres, M. Aguiló, F. Díaz, Y.C. Wang, V. Petrov, U. Griebner, E. Vilejshikova, K. Yumashev, and W.D. Chen, Crystal growth, optical spectroscopy and laser action of Tm^{3+} -doped monoclinic magnesium tungstate, submitted to *Opt. Express* (2016).
14. J. M. Serres, X. Mateos, P. Loiko, K. Yumashev, N. Kuleshov, V. Petrov, U. Griebner, M. Aguiló, and F. Díaz, Diode-pumped microchip $\text{Tm}:\text{KLu}(\text{WO}_4)_2$ laser with more than 3 W of output power, *Opt. Lett.* **39**, 4247 (2014).
15. W. B. Cho, J. H. Yim, S. Y. Choi, S. Lee, A. Schmidt, G. Steinmeyer, U. Griebner, V. Petrov, D.-I. Yeom, K. Kim, and F. Rotermund, Boosting the nonlinear optical response of carbon nanotube saturable absorbers for broadband mode-locking of bulk lasers, *Adv. Funct. Mater.* **20**, 1937 (2010).
16. Q. Bao, H. Zhang, Y. Wang, Z. Ni, Y. Yan, Z. X. Shen, K. P. Loh, and D. Y. Tang, *Adv. Funct. Mater.* **19**, 3077 (2009).
17. M. Segura, M. Kadankov, X. Mateos, M. C. Pujol, J. J. Carvajal, M. Aguiló, F. Díaz, U. Griebner, and V. Petrov, Atomic-layer graphene as a saturable absorber for ultrafast pulsed lasers, *Opt. Express* **20**, 3394 (2012).
18. H. Yu, V. Petrov, U. Griebner, D. Parisi, S. Veronesi, and M. Tonelli, Compact passively Q-switched diode-pumped $\text{Tm}:\text{LiLuF}_4$ laser with 1.26 mJ output energy, *Opt. Lett.* **37**, 2544 (2012).
19. J.M. Serres, P. Loiko, X. Mateos, K. Yumashev, U. Griebner, V. Petrov, M. Aguiló, and F. Díaz, $\text{Tm}:\text{KLu}(\text{WO}_4)_2$ microchip laser Q-switched by a graphene-based saturable absorber, *Opt. Express* **23**, 14108 (2015).
20. P. Loiko, J.M. Serres, X. Mateos, K. Yumashev, A. Yasukevich, V. Petrov, U. Griebner, M. Aguiló, and F. Díaz, Subnanosecond $\text{Tm}:\text{KLuW}$ microchip laser Q-switched by a Cr: ZnS saturable absorber, *Opt. Lett.* **40**, 5220 (2015).
21. R. Lan, P. Loiko, X. Mateos, Y. Wang, J. Li, Y. Pan, S. Y. Choi, M. H. Kim, F. Rotermund, A. Yasukevich, K. Yumashev, U. Griebner, and V. Petrov, Passive Q-switching of microchip lasers based on Ho: YAG ceramics, *Appl. Opt.* **55**, 4877 (2016).